Influence of short-range adatom-adatom interactions on the surface diffusion of Cu on Cu(111)

Mihai-Cosmin Marinica, Cyrille Barreteau, and Marie-Catherine Desjonquères
Commissariat à l'Energie Atomique, DSM/DRECAM/SPCSI, Centre d'Etudes de Saclay, F-91191 Gif sur Yvette, France

Daniel Spanjaard
Laboratoire de Physique des Solides, Université Paris Sud, Bâtiment 510, F-91405 Orsay, France
(Received 27 January 2004; revised manuscript received 26 April 2004; published 31 August 2004)

The EAM potential set up by Mishin *et al.* [Phys. Rev. B **63** 224106 (2001)] is used to study some elementary processes in the homoepitaxy of Cu on Cu(111). After having checked its ability to reproduce surface physical quantities, this potential is applied to an investigation of the energetics, the vibrations and the surface diffusion of Cu_N close-packed adislands ($1 \leqslant N \leqslant 7$). In each case we determine the most stable configurations, the corresponding activation barriers, the local vibrational spectra, and the Vineyard prefactors. In particular it is found that, at room temperature, dimers and trimers are still very mobile and move by concerted jumps much faster than tetramers while heptamers can be considered as immobile. The very good agreement of our results with scanning tunneling microscopy observations justifies the use of Mishin *et al.* potential for treating surface diffusion. This allowed us to study in details the influence of the lateral atomic environment of the adatoms along its diffusion path. An effective lateral pair interaction model is set up which is able to predict the existence of a saddle point along the path and to give a very good estimation of the activation barrier height. This model will be very useful in kinetic Monte Carlo simulations of homoepitaxial growth of Cu(111).

DOI: 10.1103/PhysRevB.70.075415 PACS number(s): 68.43.Fg, 68.43.Hn, 68.43.Jk

I. INTRODUCTION

The study and characterization of crystal growth has, apart from its theoretical interest, important implications in technology. The process of fabrication of very thin metal films is commonly used in electronics, optoelectronics, and recording media industry. The more the growth is understood, the more controlled the fabrication processes can be made and, consequently, a better quality of the device performances can be obtained.

The study of the homoepitaxial growth on fcc(111) metal surfaces has been the subject of a very large number of theoretical[1–6] and experimental[7,8] works since, in spite of its apparent simplicity, it is actually rather involved. Indeed, there are two threefold adsorption sites: the normal (f) site which continues the stacking order of (111) planes in the fcc structure and the fault (h) site which, if occupied by the adatom during a growth process, will introduce the hcp stacking order. In addition, adatom islands at equilibrium are expected to be limited by close-packed atomic rows corresponding to two different types of microfacets: (001) type for A edges and (111) type for B edges, i.e., to the two types of ledges for steps with close-packed edges on fcc(111) surfaces. Furthermore, crystal growth is a kinetic process and thus not only the most stable sites are involved, but also the diffusion barriers encountered either by a single adatom in various atomic environments or by small clusters. In particular, the critical cluster size beyond which the nuclei become immobile must be determined. Moreover, the relative diffusion rates of adatoms along steps A and B is of great importance for the growth of adislands and the knowledge of the diffusion barriers encountered for an adatom jumping between two sites at which it has nearest or next nearest neighbor lateral bonds (i.e., between two small clusters) is crucial for the description of the coalescence of two clusters.

Several works have been devoted to the determination of the preferred adsorption site of individual adatoms on fcc(111) metal surfaces. Indeed, the f and h sites, being both threefold coordinated, are expected to be very close in energy and thus their relative stability may depend on the chemical species. For instance, from field ion microscopy,[9] it has been established that an Ir atom on Ir(111) occupies a h site whereas for Pt on Pt(111) the preferred site is an f site. In addition Repp *et al.*,[10] using scanning tunneling microscopy (STM), have found that a Cu adatom on Cu(111) sits at an f site, although the h site is almost degenerate in energy. On the theoretical side, three types of methods can be used to calculate the adsorption energy: the semiempirical potentials, the tight-binding model, and *ab initio* methods based on the density functional theory. From the tight-binding approximation general trends were derived predicting the most stable adsorption sites for metals with a partially filled *d* band.[11,12] *Ab initio* methods have mainly been applied to the study of Al, although a few works have been devoted to Cu and Ag. Indeed, the numerical accuracy required to distinguish between f and h sites is very hard to achieve, in particular for transition and noble metals. Various works concerning Al (Refs. 2, 13, and 14) agree to conclude that the h site is the most stable one, the f site being almost degenerate with the bridge site. According to *ab initio* calculations for Ag (Ref. 15) and Cu (Refs. 10 and 16) the f site is very slightly preferred to the h site (by some meV) for both metals. On the contrary, when using semiempirical potentials, the numerical calculations can be as precise as needed. However, these potentials being approximate, the relative stability of f and h sites may depend on the fitting data base used as input in the determination of the potential parameters.[17] Thus the reliability and the transferability must be extensively checked. In

TABLE I. Surface relaxation of low index Cu surfaces calculated from the EAM potential and compared with experiments.

$\Delta_{ij}=\left(z_{ij}/z_{ij}^0-1\right)$	(111)		(100)		(110)	
	EAM	Expt.[a]	EAM	Expt.[b]	EAM	Expt.[c]
Δ_{12}(%)	−1.4	−0.7±0.5	−1.3	−1.2	−4.4	−8.5±0.6
Δ_{23}(%)	0.1		−0.2	0.9	0.2	2.3±0.8
Δ_{34}(%)	0.2		0.3		−0.5	

[a]Reference 28.
[b]Reference 29.
[c]Reference 30.

particular, for the present problem, it should give at least the relative stability of hcp and fcc bulk phases correctly and an accurate value for the bulk stacking fault energy. Finally, the diffusion barriers for a single adatom are rather low: for instance about 40 meV for Al and Cu, according to both theory and experiments.[10,14,18,19] This suggests that very small adislands can still be mobile.[20] A high mobility has indeed been observed in STM experiments,[10] at least for Cu dimers.

A systematic investigation of the relative stability and diffusion barriers of Al N-mers ($N=1,\ldots,5$) on Al(111) has been carried out by Chang *et al.*[14] by using the Vienna *ab initio* simulation package.[21] The state of knowledge seems to be quite different for Cu. Only a few *ab initio* results can be found in the literature for the dimer[10] and for the trimer,[16] obviously due to the numerical difficulties mentioned above. In addition, the results reported by Chang *et al.* for Cu N-mers obtained using an embedded atom method (EAM) potential are only partial. Clearly a systematic investigation of all possible displacements of dimers and trimers is still lacking for Cu. Finally, if the influence of oscillatory adsorbate-adsorbate interactions at medium range on the diffusion barriers of an adatom in the presence of a second adatom has also been investigated both for Al and Cu,[22–24] little is known about the influence of adatom-adatom interaction at short range.

We have undertaken a systematic study of the diffusion barriers encountered by Cu adatoms or very small clusters in various atomic geometries, with the purpose of finding a simple formula able to provide a good estimation of the diffusion barriers as a function of the atomic environment of the diffusing atom. The final aim is to use them as input in a kinetic Monte Carlo (KMC) code. Indeed, in this type of simulation it is quite risky to consider only a few diffusion mechanisms and, since it is obviously impossible to calculate *a priori* all of them, a simple expression is highly desired. Note however that there exists some simulation schemes going beyond standard KMC for instance the dimer method based KMC (Ref. 25) or the accelerated molecular dynamics proposed by Voter *et al.*[26] Although these methods provide an accurate description of the dynamics they are much more computationally demanding than usual KMC. Indeed the latter method allows one to simulate long time scale processes much faster especially when a simple expression is available to estimate barriers.

While the barriers that we plan to calculate could be possibly computed *ab initio* in the case of Al, this would require terribly lengthy calculations for Cu, since, even in the most recent calculations,[10] the energy differences are strongly sensitive to the k-point sampling and it is not obvious that the convergence is completely achieved. Furthermore, it is doubtful that the results obtained for Al can be transferred, even qualitatively, to Cu. Indeed, even in the case of a single adatom, Al and Cu behave differently since, from the *ab initio* data reported above, the diffusion proceeds by h-h-h jumps for Al and by f-h-f jumps for Cu. As a consequence, in the following, the energetics and dynamics of Cu is described using the potential derived by Mishin *et al.*[27] which satisfies the requirement of giving the correct bulk stacking of (111) planes. After presenting very briefly this potential and checking its transferability (Sec. II) by calculating various surface properties, we study the adsorption and diffusion properties of monomers, dimers, trimers, tetramers, and heptamers (Sec. III), the aim being twofold: first, to provide additional tests for the potential by a detailed comparison with existing theoretical and experimental data and, second, to complete these data. Finally in Sec. IV the influence of short range adatom-adatom interactions on the diffusion of a single atom is investigated and an approximate formula for the diffusion barriers is derived which will be very useful for KMC simulations. Conclusions are drawn in Sec. V.

II. THE EMPIRICAL POTENTIAL

The potential derived by Mishin *et al.*[27] for copper is based on the EAM. In this model the total energy of an assembly of N atoms is written as a function of all interatomic distances r_{ij}:

$$E_{\mathrm{tot}}=\frac{1}{2}\sum_{i,j=1}^{N}V(r_{ij})+\sum_{i=1}^{N}F(\rho_i), \tag{1}$$

with

$$\rho_i=\sum_{j\neq i}\rho(r_{ij}), \tag{2}$$

where the pair potential $V(r)$, $\rho(r)$, and $F(\rho)$ are fitting parametrized functions which, on the whole, contain 28 parameters. The analytical expressions of $V(r),\rho(r)$, and $F(\rho)$ and the corresponding values of the optimized parameters can be found in Ref. 27.

Mishin *et al.* have tested their potential on many physical quantities not included in the fitting data base. These quan-

TABLE II. Step energies ($E_{step}^{A(B)}$), kink energies ($E_{kink}^{A(B)}$), stable and unstable stacking fault energies in the bulk (γ_{SF}, γ_{us}) and at the surface (γ_{SF}^{surf}, γ_{us}^{surf}) calculated from the EAM potential and compared with available experiments.

	EAM (eV)	Experiments (eV)
E_{step}^{A}	0.263	0.220±0.02[a]
E_{step}^{B}	0.265	0.220±0.02[a]
E_{kink}^{A}	0.137	0.113±0.008[b]
E_{kink}^{B}	0.134	0.121±0.008[b]
γ_{SF}	0.015	0.016[c]
γ_{us}	0.055	
γ_{SF}^{surf}	0.007	
γ_{us}^{surf}	0.061	

[a]Reference 31.
[b]Reference 32.
[c]Reference 33.

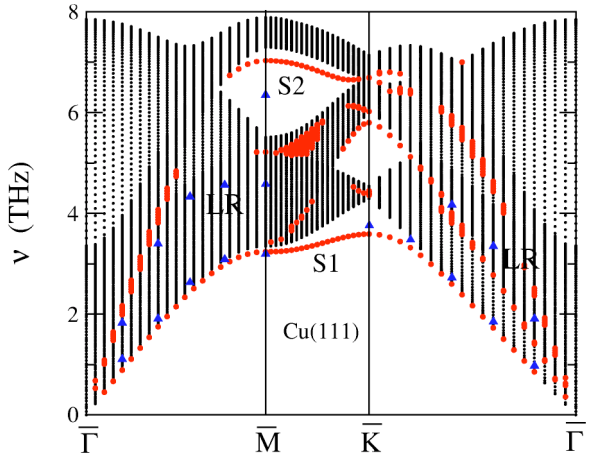

FIG. 1. The surface projected phonon band structure of Cu(111) along high symmetry lines of the Brillouin zone calculated using the EAM potential. S1, S2, and LR are surface or resonant modes. Experimental data (full triangles) are taken from Ref. 34.

ties were mainly related to the properties of three-dimensional structures: phonon spectra, point and planar defects, relative stability of different phases and deformation paths between them. However, save for the calculation of surface energies of the three low index surfaces [(111), (100), and (110)], no other surface properties have been checked. For this purpose we have determined the surface relaxation of these surfaces (Table I), the step and kink energies at 0 K of the vicinal surfaces with (111) terraces and close-packed step edges, i.e., $p(111)\times(100)$ (A step) and $p(111)\times(\bar{1}11)$ (B step) in the limit $p\rightarrow\infty$ (in practice $p=20$) in the usual Somorjai notations (Table II). In addition, the surface projected phonon band structure of Cu(111) has been determined and compared with experiments[34] (Fig. 1). The overall agreement with other theoretical or experimental data is quite satisfactory and shows that this potential is reliable for surface simulations. Note that, compared to many other existing semiempirical potentials for Cu, it has the advantage of giving the correct relative stability of the fcc and hcp structures and the bulk stacking fault (SF) energy which are essential for the present study, as already stated above. We have also verified that the surface plane obeys the regular fcc stacking. The energy profile ΔE (relative to the fcc stacking) when the surface atomic layer is shifted from fcc stacking to a surface hcp stacking is given in Fig. 2 compared with the corresponding profile for the intrinsic bulk SF. Note that the SF energy decreases at the surface (see Table II) while the energy at the saddle point (unstable SF) increases.

III. EQUILIBRIUM STRUCTURE AND DIFFUSION OF VERY SMALL ADISLANDS OF Cu ON Cu(111)

A. The adsorption geometry

As stated in the Introduction, the (111) surface presents two types of adsorption sites (Fig. 3): the normal sites (f) and the fault sites (h). These sites being both ternary they are expected to have similar binding energies and they can be simultaneously occupied.

There are obviously at least two geometries for the dimer (Fig. 3): either both atoms are at f nearest neighbor sites (ff dimer) or both are at h nearest neighbor sites (hh dimer). However a third geometry might be possible in which an atom is at an f site and the other one at the next nearest h site (fh dimer). In this latter case and in the absence of atomic relaxation, the bond length of the dimer is expanded by only 15% but this expansion may be reduced by relaxation effects as we will see in the following.

For triangular closed-packed trimers we must distinguish between trimers in which the center of the cluster is above an atom or at an adsorption site of the surface layer. In the first case, the clusters have (100)-type microfacets and we will denote them as A-trimers by analogy with the usual notation for the corresponding steps with (111) terraces. In the second case the trimers have (111)-type microfacets and will be denoted as B-trimers. In both cases all atoms in the trimer can sit either at f or at h sites. Note that A-trimers interact directly with 7 atoms of the surface forming a regular hexagon while B-trimers have bonds with 6 atoms of the substrate arranged in an equilateral triangle. Thus four types of trimers

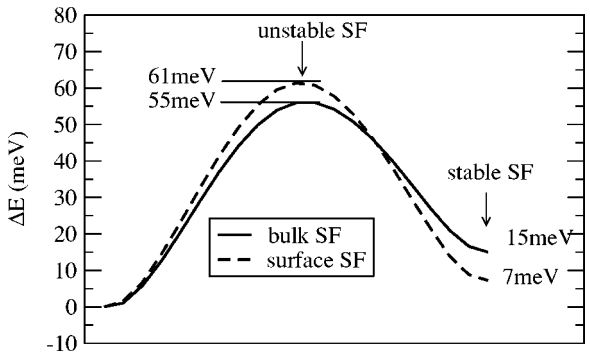

FIG. 2. The energy profile when a stacking fault is created by shifting one half of the crystal (bulk SF) relative to the other along the (111) plane or the (111) surface layer (surface SF) in the $\langle\bar{2}11\rangle$ direction.

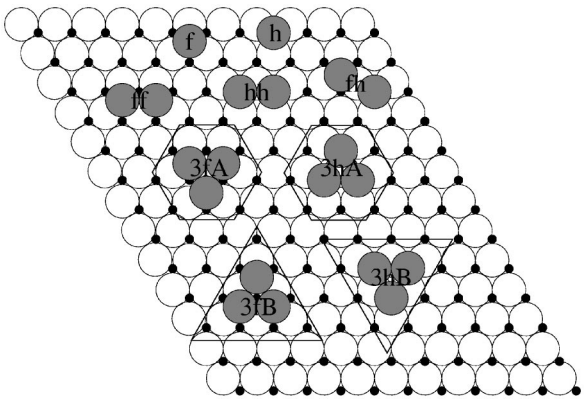

FIG. 3. The various geometrical configurations of monomers, dimers, and triangular trimers on the (111) surface of fcc crystals. The open interstices (black dots) correspond to f(h) sites.

will be considered in the following: 3fA, 3hA, 3fB, 3hB (Fig. 3).

In this section we study the equilibrium structure, diffusion barriers and vibrational spectrum of these small adislands and compare the results with existing theoretical and experimental data. The next subsection is devoted to a brief presentation of the calculation methods giving access to these properties.

B. Calculation methods

1. The determination of the equilibrium structure

The algorithm used to relax the atomic geometry is based on a *damped* molecular dynamics.[2,35] In a finite-difference form the time evolution of any atomic position $\mathbf{R}_i$ is given by

$$\mathbf{R}_i(n+1) = \mathbf{R}_i(n) + \lambda[\mathbf{R}_i(n) - \mathbf{R}_i(n-1)] + \mu \mathbf{F}_i(n), \quad (3)$$

where $\mathbf{R}_i(n)$ is the position of atom i and $\mathbf{F}_i(n)$ the force acting on it at the nth time step. The parameters λ and μ are chosen so that the evolution of the atomic positions leads rapidly to the nearest local minimum of E_{tot} and avoids oscillations around it. Convergence is achieved at the mth iteration step when $\mathrm{Sup}_i|\mathbf{F}_i(m)| < 10^{-3}$ eV/Å. For Cu adatoms on Cu(111) a fast convergence is obtained with $\lambda = 0.5$ and $\mu = 0.1$ Å^2/eV. Usually a few tens of iterations are enough to converge to the required accuracy.

2. The determination of diffusion barriers

The determination of the diffusion barriers has been carried out by means of the Ulitsky-Elber algorithm.[36] Let us briefly recall the principle of this technique. The problem is to find the saddle point between two stable (or metastable) configurations $\mathcal{C}$ and $\mathcal{C}'$. The most simple guess for a diffusion path is to take a linear interpolation between these two configurations. This initial guess, which is most often quite poor, is iteratively refined until the minimum barrier height is reached. For this purpose this initial path is discretized into N_p+1 configurations and is distorted by moving each atom in each configuration according to Eq. (3) in which the force $\mathbf{F}_i$ is replaced by its component perpendicular to the path, $\mathbf{F}_{i,\perp}$. The process is iterated until all the forces $\mathbf{F}_{i,\perp}$ vanish. The maximum value of E_{tot} along the final path gives the saddle point since the energy has been minimized except in the direction of the path. In practice we have taken $N_p = 14$ and stopped the iteration process when $\mathrm{Sup}_i|\mathbf{F}_{i,\perp}| < 10^{-2}$ eV/Å.

3. The determination of the adatom(s) vibration spectrum

Two methods have been used to study the vibrational properties of adatom(s): the diagonalization of the dynamical matrix in the harmonic approximation (HA) and the molecular dynamics (MD). In the HA, the local spectral vibration density (LSVD) of atom i in the direction α ($\alpha = x,y,z$) is defined as[37]

$$n_{i\alpha}(\nu) = \sum_n |u_{i\alpha}(\nu_n)|^2 \delta(\nu - \nu_n), \quad (4)$$

where $u_{i\alpha}(\nu_n)$ is the component on atom i and direction α of the normalized eigenvector of the dynamical matrix corresponding to the eigenfrequency ν_n. In MD the LSVD of atom i in direction α is obtained from the velocity autocorrelation function:[38,39]

$$S_{i\alpha}(\nu) = \int_0^\infty dt\, e^{i2\pi\nu t} \langle V_{i\alpha}(t) \cdot V_{i\alpha}(0) \rangle, \quad (5)$$

where $V_{i\alpha}(t)$ is the velocity of atom i projected on the direction α at time t. If the potential were strictly harmonic, the two quantities $n_{i\alpha}(\nu)$ and $S_{i\alpha}(\nu)$ (when properly normalized) are equal. However in a realistic potential $S_{i\alpha}(\nu)$ takes anharmonic effects into account, the latter increasing with temperature. In both methods the LSVD on a given site is obtained by averaging over the three directions α.

Let us present some computational details of the MD simulation. The classical equations of motion were integrated using the Verlet algorithm in its velocity-velocity form[40] with a time step of 3 fs. Unless otherwise stated, the simulation box is built from 20 layers with (111) orientation, each layer containing 121 atoms (i.e., 11×11 atoms). For each layer we applied periodic boundary conditions in the XY plane perpendicular to the $\langle 111 \rangle$ direction. On the surface of this slab adatoms are added. The system is equilibrated for about

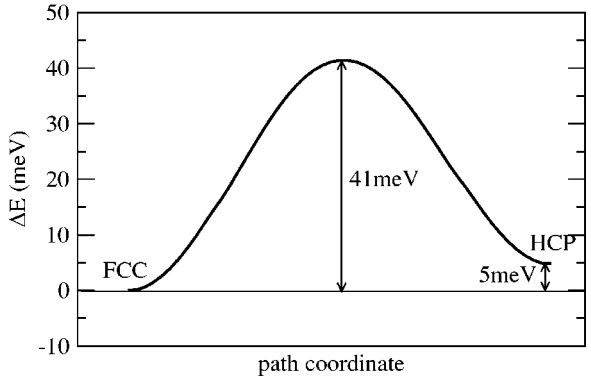

FIG. 4. The potential energy profile encountered by a Cu adatom diffusing from an f site to an adjacent h site on the Cu(111) surface.

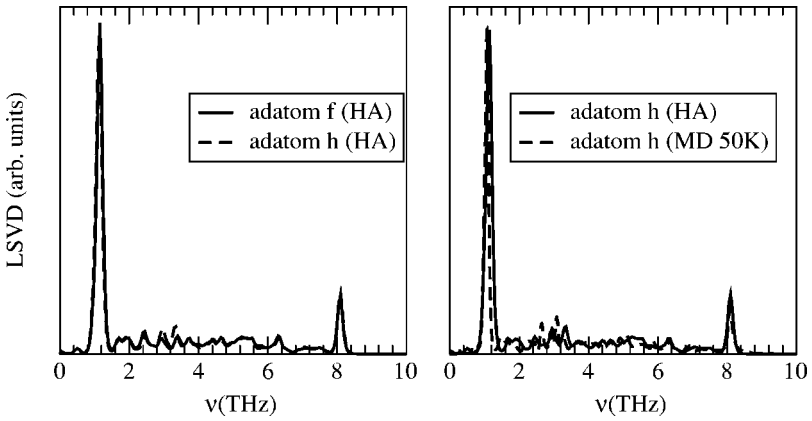

FIG. 5. Left-hand side: local spectral vibration densities (LSVD) averaged over the three directions on an isolated Cu adatom at f and h sites on Cu(111) from the harmonic approximation (HA). Right-hand side: comparison of the LSVD obtained from harmonic approximation and molecular dynamics (MD) for an adatom at an h site.

10 ps and the physical information is extracted during another period of about 80 ps of simulation in the μ-canonical (NVE) ensemble.[38] During this last stage of calculation the drift in the total energy of the system was less than 10^{-4}% and the ratio of the root mean square fluctuations $\sigma(E)$ of the total and kinetic energy $\sigma(E_T)/\sigma(E_K)$ was always less than 2%. The Fourier transform of Eq. (5) was computed using a Fast Fourier Transform algorithm with 16384 points. Hence the precision in the calculated spectra is estimated to be about 3×10^{-2} THz.

C. Results

As a preliminary study we have performed a molecular dynamic calculation at 300 K to follow the evolution of 52 adatoms distributed randomly at the surface of a slab of (111) orientation. The slab is built from a 25×25 supercell geometry with 30 layers. After 15 ns no single adatom remains on the surface, they are all associated in dimers, trimers, etc. As expected these small islands are far from being motionless and diffusion of dimers and trimers at very short time scale is observed. This suggests the existence of small energy barriers for the concerted motion of these small adislands, which subsequently recombine into larger islands. Moreover one never observes the dissociation of a dimer or a trimer suggesting that the associated bond breaking energy is much larger than the energy of concerted rotation or translation.

In the following we will analyze the possible movements of monomers, dimers, and trimers with their associated energy path.

1. Monomer

Let us start with the case of an isolated Cu adatom. It is found that the most stable adsorption site is an f site, however the h site is only slightly less stable (by 5 meV, see Fig. 4). Thus the elementary movement is a hopping from an f to an h site. In Fig. 4 we have plotted the minimum energy path of the f$\leftrightarrow$h motion. The energy barrier $E_{\mathrm{f}\rightarrow\mathrm{h}}$ is extremely small since its value is only 41 meV. These results are in perfect agreement with the recent experimental data of Repp *et al.*[10] who estimate the energy barrier at $E_{\mathrm{f}\rightarrow\mathrm{h}}=37\pm5$ meV and find an h/f energy difference ranging between 4 and 8 meV.

In addition we have calculated the LSVD on the adatom in f and h sites. In Fig. 5 we show the result of our HA and MD calculations at 50 K. The agreement between the two methods is almost perfect, apart from a very small shift towards lower frequencies at the bottom of the spectrum, observed in MD as predicted by the first nonzero correction to harmonicity.[41] This correction is negative and varies as $1/v^4$ thus, rapidly vanishes when ν increases. There are two strik-

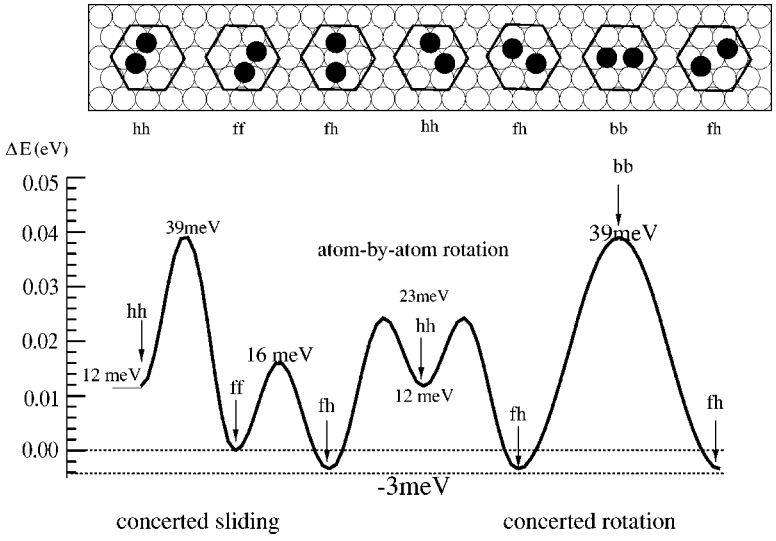

FIG. 6. Schematic illustration of intracell, i.e., nondiffusive dimer motion and the corresponding energy profile.

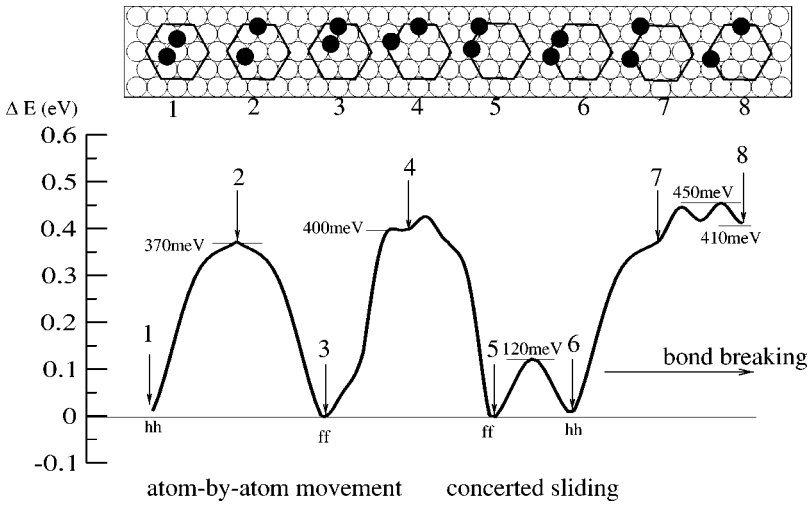

FIG. 7. Schematic illustration of intercell dimer motion leading to diffusion or dissociation and the corresponding energy profile.

ing features in the LSVD: first the perfect similarity of the f and h spectra, and second the presence of two narrow peaks around 1 THz and 8 THz. An analysis of the polarization shows that the low frequency peak corresponds to oscillations in the plane of the surface (for which the corrugation of the potential is very small) while the high frequency one is polarized along the normal to the surface.

2. Dimer

The dimer motion is more complicated since, in addition to ff and hh dimers separated by $d_1 = 2.55$ Å with bonds pointing in a close-packed direction, there is also a dimer in an fh configuration with a bond length $d_2 = 2.95$ Å (see Fig. 3). In the following, two atoms separated by d_1 will be called nearest neighbors (nn), while atoms separated by d_2 (in the absence of relaxation) will be called "pseudo" nearest neighbors (pn). For the unrelaxed system the energy of the fh dimer is higher by 150 meV than that of the ff dimer. When relaxation is allowed this energy difference totally disappears and the mixed fh dimer even becomes slightly favored by about 3 meV with respect to ff dimers, while the energy of hh dimers is 12 meV higher than that of ff dimers. This mixed dimer ground state, previously described by Bogicevic *et al.*[42] in the context of Al dimer dynamics on Al(111), is attributed to a strong contraction of the dimer bond length. Indeed due to relaxation the bond-length of the mixed dimer is shortened by 16% and finally ff, hh, and fh dimers have almost the same bond length (around 2.45 Å). Experimentally the ff dimer is found to be very slightly favored by about 1 meV with respect to fh.[10]

TABLE III. Diffusion barriers and corresponding attempt frequencies for concerted *diffusive motions* of Cu_N adislands on Cu(111): ▶ from f to h sites (3fA→3hB for Cu_3), ◀ from h to f sites (3hB→3fA for Cu_3). For Cu_4 the letters D and O refer to the diagonal and oblique motion, respectively.

Adisland	Cu	Cu_2	Cu_3	Cu_4(D)	Cu_4(O)	Cu_7
Barrier(meV)						
▶	41	132	155	262	189	388
◀	36	120	133	238	165	346
ν_0(THz)						
▶	1.14	1.32	4.51	4.12	4.65	13.17
◀	1.16	1.40	6.47	5.05	5.70	18.00

The dimer motion can be classified into two categories: intracell and intercell motions. In the former case the dimer is confined inside a small hexagon (Fig. 6) and the motion is nondiffusive, whereas in the latter there is a diffusion out of the hexagon (Fig. 7).

Let us first examine the intracell motion which is the most frequently observed in the molecular dynamic simulation. The motion in the hexagonal cell can proceed by (i) concerted sliding ff↔hh, (ii) atom-by-atom rotation around the central atom of the hexagon ff↔fh↔hh, or (iii) concerted rotation fh↔bb↔fh where bb is the bridge configuration (see Fig. 6). The lowest energy barrier is obtained for the atom-by-atom rotation ff→fh which is only 16 meV, in perfect agreement with the experiments of Repp *et al.*[10] from which an intracell-diffusion barrier of 18±3 meV is deduced. In contrast the energy barrier fh→hh is 26 meV, this implies that, at very low temperature, the dimer will spend more time going back and forth between ff and fh configurations than doing the full rotation. Finally, concerted sliding and rotation have diffusion barriers of the same order of magnitude as for the isolated adatom.

The intercell motion is made of (i) atom-by-atom motion and (ii) concerted sliding (Fig. 7). In the atom-by-atom motion one of the atom is trying to break the dimer bond which needs to overcome a barrier of the order of 400 meV. Moreover if this motion is made of a single f↔h jump the final configuration is unstable. In this particular case the atomic relaxation has been allowed only along the *z* direction in order to avoid complex concerted motions. The dissociation energy of the dimer is around 450 meV and, consequently, diffusion will be largely dominated by concerted sliding that costs only 120 meV, still four times larger than for the intracell motion. Let us also mention that if lateral relaxation is allowed the energy cost of a concerted sliding is slightly modified (132 meV instead of 120 meV, see Table III).

In addition we have calculated the LSVD on the dimer, both within HA and MD. The LSVD on the ff and fh dimers

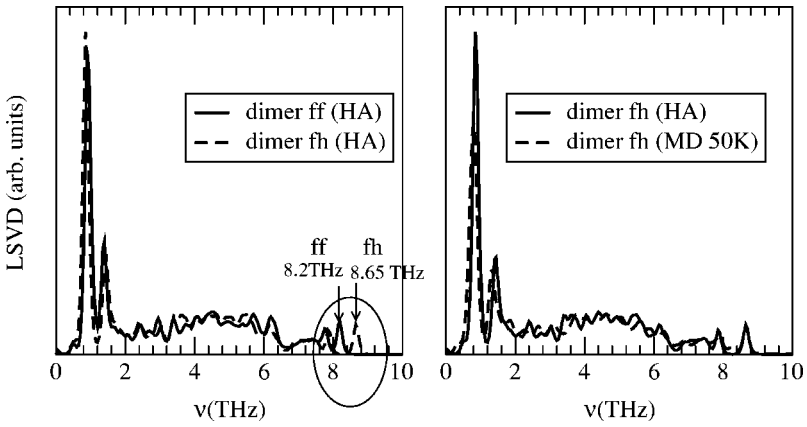

FIG. 8. Same caption as in Fig. 5 for Cu adatoms belonging to a dimer. Note that the LSVD of both atoms of an fh dimer are almost indistinguishable.

(Fig. 8) are very similar apart from an upward shift of the high frequency peak at 8.2 THz for the ff dimer and at 8.65 THz for the fh dimer. This peak is associated to a purely vertical motion. The agreement between MD and HA is almost perfect at 50 K. A shift towards low frequencies at the bottom of the spectrum, due to anharmonic effects and similar to that calculated for monomers, is found in MD. In Fig. 9 we have also compared the LSVD at 50 and 300 K, showing two clear behaviors: as the temperature rises the high frequency peak disappears, and the low frequency peak is shifted towards zero. This can be quite simply understood since, when the temperature increases, the dimer diffuses rapidly in the plane of the surface and never stays enough time at the same lateral position to explore the vertical dependence of the potential. Consequently it cannot be reproduced in the simulation. Moreover since the planar motion is extremely easy due to the very small corrugation of the potential as already stated, a very low frequency motion in the plane of the surface is possible at room temperature.

3. Trimer

For the motion of trimers we have only considered concerted motion since atom-by-atom movement is very unlikely, the energy to break a bond being much larger (see Sec. IV) than the energy barrier involved in a concerted motion. The energetically most favorable configuration is the 3fA triangle, while 3fB, 3hA, and 3hB are, respectively, 5 meV, 17 meV, and 22 meV higher in energy (see Fig. 10). It is interesting to note that, even at this size, A edges are favored with respect to B edges.

A typical sequence of motion develops as follows (see Fig. 10): a 3hB triangle transforms into a 3fA triangle by a concerted translation, a concerted rotation then leads to a 3hA triangle which transforms into a 3fB triangle by another concerted translation. The energy barrier involved in the nondiffusive motion is slightly smaller (concerted rotation: 111 meV) than the one involved in the diffusive mechanism (concerted translation: 155 meV).

4. Tetramer and heptamer

We have also considered the motion of a diamond shape tetramer and a hexagonal close-packed heptamer. The tetramer has two types of diffusion processes from a regular fcc stacking to a faulted hcp stacking by concerted sliding: one motion in the direction of the long diagonal of the diamond (denoted diagonal motion) and two equivalent oblique motions (see Fig. 11). A truly diffusive motion cannot proceed by only diagonal motions, however diagonal-oblique and oblique-oblique motions are both possible. The energy profile along a diagonal-oblique path is shown in Fig. 11. The oblique motion is lower in energy (189 meV from f to h, 165 meV from h to f) than the diagonal one (262 meV from f to h, 238 meV from h to f), as a consequence oblique-oblique motions are energetically favorable. The motion of the heptamer is simpler since hexagonal adislands have a threefold symmetry and the three possible movements from f to h sites are equivalent. The diffusion barrier to be over-

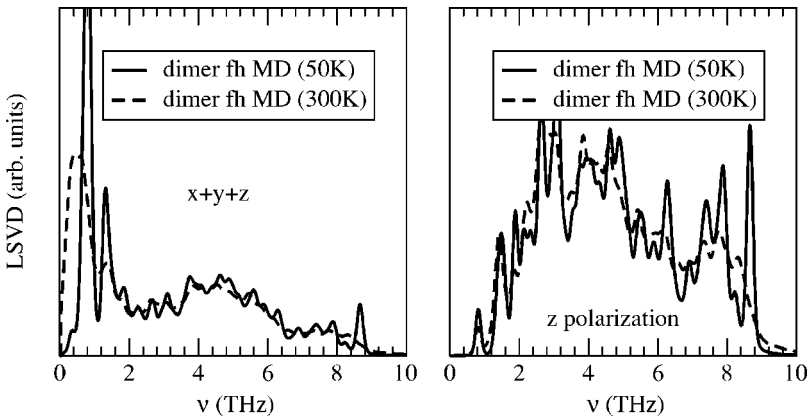

FIG. 9. The local spectral vibration density on an fh dimer from molecular dynamic (MD) calculations at 50 K and 300 K averaged over the three directions (left-hand side) and in the *z* direction (right-hand side).

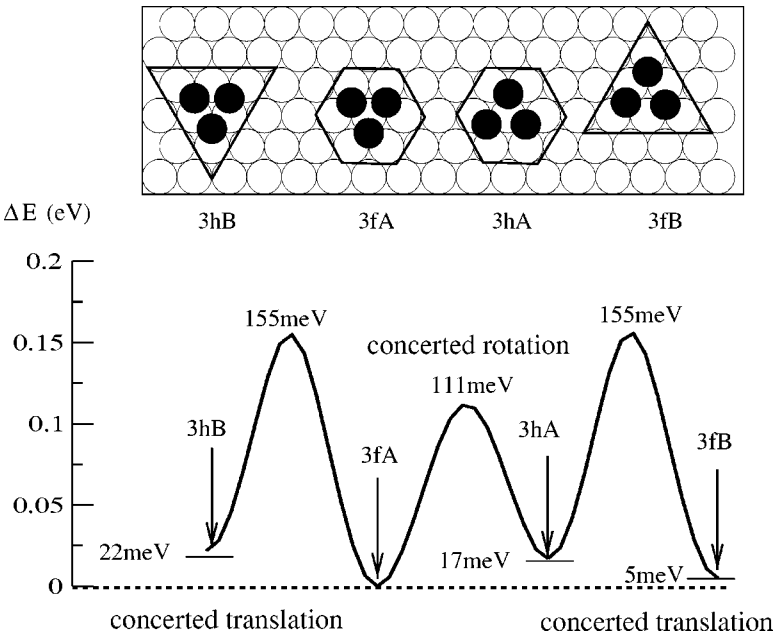

FIG. 10. Schematic illustration of trimer concerted motion and the corresponding energy profile.

come is 388 meV from f to h and 346 meV from h to f, showing that such adislands can still be mobile at moderate temperatures.

Finally let us comment on the relative stability of f sites with respect to h sites and the corresponding energy barriers. It is quite interesting to note that the energy difference per atom between f and h sites $E_h - E_f$ [where E_h and E_f are the total energy of the system with adatom(s) at h and f sites, respectively] is almost independent on the adisland size. This quantity is equal to 5 meV for a monomer, 6 meV for a dimer, 5–6 meV for a trimer, 6 meV for a tetramer, 6 meV for an heptamer, and finally 7 meV for a complete layer (see Table II).

In contrast the energy barrier per atom $E_{f\to h}$ is more sensitive to the size and the geometry since it is equal to 40 meV for a monomer, 20 meV for the nondiffusive motion of a dimer, and 66 meV for its diffusive motion, 52 meV (concerted translation) for a trimer, 65 meV and 47 meV for the diagonal and oblique motion of the tetramer, respectively, and 55 meV for the heptamer. These figures should be compared to the 61 meV energy barrier needed to shift a complete surface layer from fcc to hcp stacking (see Table II and Fig. 2).

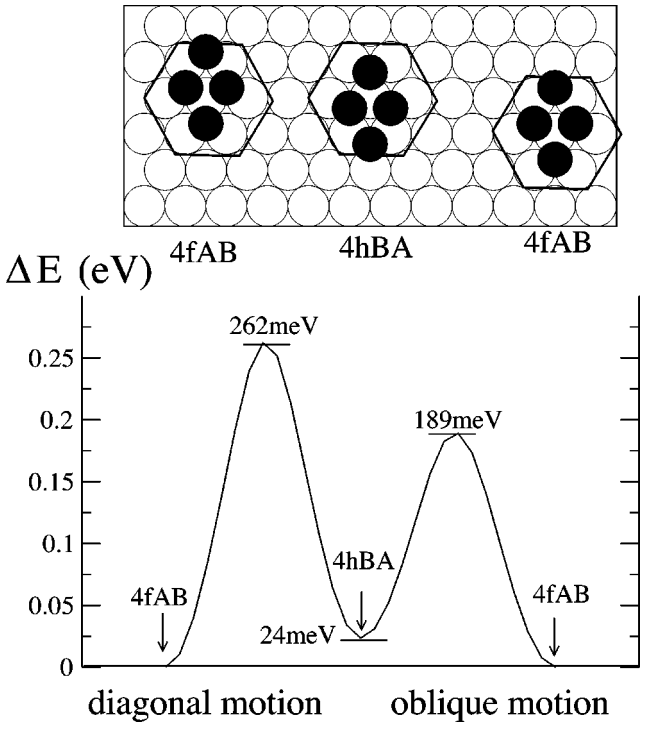

FIG. 11. Schematic illustration of tetramer concerted motion and the corresponding energy profile.

5. Energy barriers and Vineyard prefactors

The knowledge of the vibrational spectrum gives also access to the attempt frequency ν_0 of the diffusion prefactor. Indeed, assuming a classical harmonic solid, the attempt frequency is given by the Vineyard's product formula.[43]

$$\nu_0 = \frac{\prod_{p=1}^{3N} \nu_p^e}{\prod_{p=1}^{3N-1} \nu_p^s} \tag{6}$$

if we call ν_p^e and ν_p^s the (real) eigenfrequencies for the equilibrium and saddle point configurations and N the total number of atoms. In Table III we have summarized the attempt frequencies together with the corresponding energy barriers, for the various diffusive motions of a monomer, dimer, trimer, tetramer, and heptamer.

The attempt frequency for the diffusion of a monomer from an f to an h site is equal to 1.14 THz while for the reverse trajectory it is 1.16 THz, as expected from the very similar LSVD on the adatom in f and h sites. These values are in very good agreement with experiments.[44] Note that the

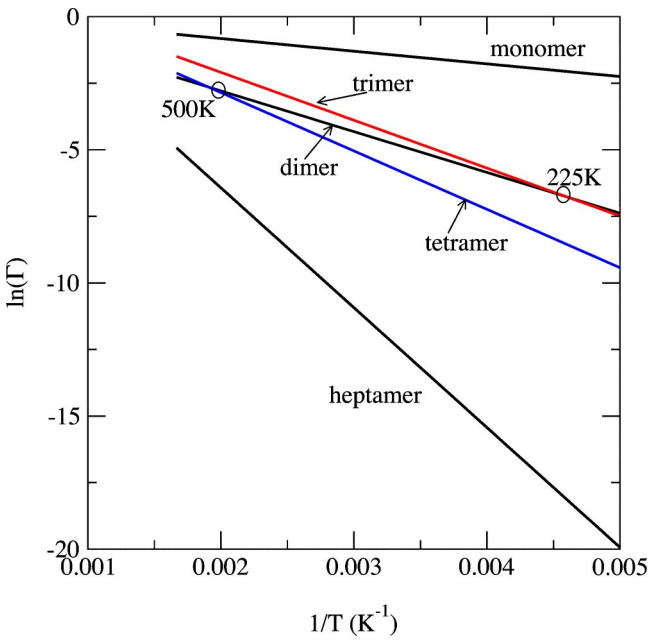

FIG. 12. Arrhenius plots of the hopping frequencies of Cu adislands for f→h diffusive motions. The tetramer straight line refers to the oblique motion.

attempt frequency does not always increase with the energy barrier, i.e., the so called Meyer-Neldel compensation effect[45] is not systematically obeyed. For instance, for each of the studied adislands sizes, the h→f motion has a higher attempt frequency than the f→h motion while the barrier is smaller, in contradiction with the expected trend. On the contrary there is a tendency for prefactors to grow simultaneously with the barrier height when the number of atoms involved in the concerted sliding increases.

The barrier heights and the attempt frequencies being known, it is easy to compare the typical time scale (or hopping frequency) of the diffusive motion as a function of the island size and temperature in order to estimate the critical number of atoms beyond which the nuclei can be considered as immobile at a given temperature. For this purpose we show in Fig. 12 the Arrhenius plots of the hopping frequencies Γ given by the harmonic transition state theory, i.e., $\Gamma = \nu_0 \exp(-\Delta E/k_B T)$, where ΔE is the barrier height. It can be seen that for instance at room temperature the monomer hopping frequency is of course the largest (corresponding to a typical time scale of $\Gamma^{-1} \simeq 4$ ps), more surprisingly the dimer and trimer have hopping frequencies of the same order of magnitude ($\Gamma^{-1} \simeq 100$ ps), the tetramer is much less mobile while the heptamer can be considered as an immobile nuclei.

IV. DIFFUSION OF AN ADATOM IN THE PRESENCE OF SMALL ADISLANDS

In most KMC simulations of homoepitaxial growth on Cu(111), the jump of an adatom from an f site to the nearest h site (or vice versa) is not considered, even though we have seen previously that this jump is the elementary process in the diffusion of very small adislands. This point of view is justified when the adislands are large enough and limited by close-packed steps for which the most important event in the growth process is the diffusion along the steps which proceeds by f-f (h-h) elementary jumps for adislands at f(h) sites.[46] However, f-h jumps may still exist in particular when the shape of the adislands is not so regular and are obviously crucial when two adislands, respectively at f and h sites, coalesce. The energy barriers $E_{f\to h}$ and $E_{h\to f}$ are expected to vary significantly with the lateral environment of the diffusing adatom. In principle, the diffusion barrier should be calculated for each configuration of adatoms but this would lead to prohibitive computer time in KMC simulations. Thus, there is a need for a simple formula giving a reasonable estimation of the energy barrier as a function of the number of neighboring adatoms. For this purpose, we must first compute a large data set of diffusion barriers, second fit these results by a simple formula and, finally, check that this formula is able to reproduce correctly a number of diffusion barriers not included in the fitting data set.

Consequently, we have calculated the initial ($E_{tot}\{\mathcal{C}\}$) and final ($E_{tot}\{\mathcal{C}'\}$) total energies as well as the diffusion barriers (when existing) corresponding to the 32 atomic geometries shown in Fig. 13. In all cases an adatom is displaced from an f site (configuration $\mathcal{C}$) to an adjacent h site (configuration $\mathcal{C}'$). The atomic geometries are labelled by two digits and a letter, the first and second digits being the number of nn bonds (of length d_1) of the displaced adatom in the initial ($N^{f}_{d_1}$) and final ($N^{h}_{d_1}$) states, respectively. The letter labels the various configurations with the same digits. Save for the displaced adatom, the calculations were carried out by assuming that all other adatoms are at strictly threefold sites, i.e., only normal relaxation has been allowed. Actually we want to mimic the displacement of an adatom in the presence of compact adislands larger than those shown in Fig. 13 in which case the adisland lateral atomic positions are somewhat fixed. Moreover it is expected that the diffusion barrier is only sensitive to the close environment (i.e., nn and pn bonds, see Sec. III C 2) in the initial and final positions. Indeed if all atoms were free to move, the optimization of the diffusion path would lead to collective motions transforming the adisland into a more compact form. In Table IV the corresponding values of $\Delta E_{fh} = E_{tot}\{\mathcal{C}\} - E_{tot}\{\mathcal{C}'\}$ are given. When a saddle point has been found (configuration $\mathcal{C}^*$) between $\mathcal{C}$ and $\mathcal{C}'$ the diffusing atom has been fully relaxed at f and h sites and the corresponding energy barriers $E_{f\to h}$ are listed. In the opposite case, either $\mathcal{C}(\Delta E_{fh} > 0)$ or $\mathcal{C}'(\Delta E_{fh} < 0)$ is unstable and only the z coordinate of the displaced atom has been optimized at f and h sites which are then rigorously threefold. Note that the diffusion barriers corresponding to the reverse diffusion (h→f) is given by

$$E_{h\to f} = \Delta E_{fh} + E_{f\to h} \tag{7}$$

which ensures the detailed balance condition. From Table IV it is obvious that neither ΔE_{fh} nor $E_{f\to h}$ is only determined by $N^{f}_{d_1}$ and $N^{h}_{d_1}$ (compare, for instance, the results for all the atomic geometries labeled 21 or 22). If we now take into account the number of pseudo-neighbors (of bond length d_2) of the displaced atom in the initial ($N^{f}_{d_2}$) and final ($N^{h}_{d_2}$)

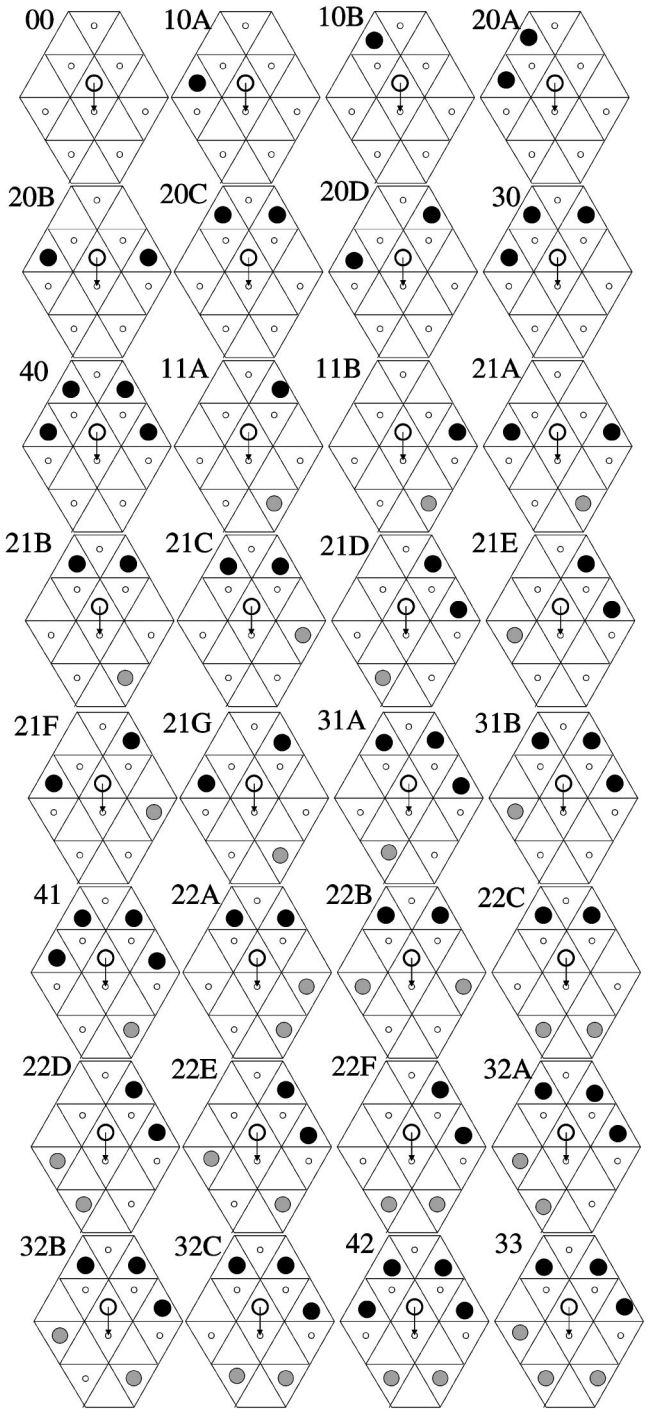

FIG. 13. The 32 atomic configurations for which the energy profile of an adatom (open circle) jumping from an f to a nearest h site has been calculated. Full black circles denote adatoms at f sites. The h sites are denoted as small open circles replaced by full gray circles when occupied by adatoms.

states, a reasonable correlation between the set of numbers $(N^{\mathrm{f}}_{d_1}, N^{\mathrm{f}}_{d_2}, N^{\mathrm{h}}_{d_1}, N^{\mathrm{h}}_{d_2})$ and ΔE_{fh} or $E_{\mathrm{f}\to\mathrm{h}}$ is observed. For instance, among the geometries labeled 21, two couples of configurations are characterized by the same numbers of nn and pn bonds: 21D and 21G, on the one hand, 21E and 21F on the other hand, and each of these couples have comparable values of ΔE_{fh} and $E_{\mathrm{f}\to\mathrm{h}}$. Moreover when $N^{\mathrm{f}}_{d_1} = N^{\mathrm{h}}_{d_1}$ and $N^{\mathrm{f}}_{d_2} = N^{\mathrm{h}}_{d_2}$, ΔE_{fh} is always very small and of the same order of magnitude as for an isolated adatom (atomic geometry 00). Finally, when $(N^{\mathrm{f}}_{d_1}, N^{\mathrm{f}}_{d_2})$ is interchanged with $(N^{\mathrm{h}}_{d_1}, N^{\mathrm{h}}_{d_2})$ it is expected that the difference in energy between the initial and final states should change sign while keeping almost the same numerical value whereas the diffusion barriers $E_{\mathrm{f}\to\mathrm{h}}$ and $E_{\mathrm{h}\to\mathrm{f}}$ should be interchanged. This is reasonably verified for the geometries 22A and 22F.

Thus, assuming that lateral relaxation effects are small, the energy difference ΔE_{fh} can be fitted with the following expression:

TABLE IV. The calculated difference $\Delta E_{\mathrm{fh}} = E_{\mathrm{f}} - E_{\mathrm{h}}$ between the initial and the final total energies and the diffusion barriers $E_{\mathrm{f}\to\mathrm{h}}$ (when existing) for a Cu adatom jumping from an f to an h site for the 32 adatom environments shown in Fig. 13. All energies are in meV. The coordination numbers corresponding to the two shortest bond lengths in the f $(N^{\mathrm{f}}_{d_1}, N^{\mathrm{f}}_{d_2})$, h $(N^{\mathrm{h}}_{d_1}, N^{\mathrm{h}}_{d_2})$, and bridge $(N_{d_1^*}, N_{d_2^*})$ sites are also listed.

Event		$(N^{\mathrm{f}}_{d_1}, N^{\mathrm{f}}_{d_2}) \to (N^{\mathrm{h}}_{d_1}, N^{\mathrm{h}}_{d_2})$	ΔE_{fh}	$N_{d_1^*}$	$N_{d_2^*}$	$E_{\mathrm{f}\to\mathrm{h}}$
1	00	$(0,0)\to(0,0)$	−5	0	0	41
2	10A	$(1,0)\to(0,1)$	−137	1	0	
3	10B	$(1,0)\to(0,0)$	−372	0	1	
4	20A	$(2,0)\to(0,1)$	−430	1	1	
5	20B	$(2,0)\to(0,2)$	−249	2	0	
6	20C	$(2,0)\to(0,0)$	−670	0	2	
7	20D	$(2,0)\to(0,1)$	−430	1	1	
8	30	$(3,0)\to(0,1)$	−741	1	2	
9	40	$(4,0)\to(0,2)$	−802	2	2	
10	11A	$(1,0)\to(1,0)$	−6	0	2	173
11	11B	$(1,0)\to(1,1)$	209	1	1	
12	21A	$(2,0)\to(1,2)$	92	2	1	
13	21B	$(2,0)\to(1,0)$	−308	0	3	379
14	21C	$(2,1)\to(1,0)$	−519	1	2	
15	21D	$(2,0)\to(1,1)$	−55	1	2	140
16	21E	$(2,1)\to(1,1)$	−350	2	1	
17	21F	$(2,1)\to(1,1)$	−350	2	1	
18	21G	$(2,0)\to(1,1)$	−55	1	2	150
19	31A	$(3,0)\to(1,1)$	−345	1	3	361
20	31B	$(3,1)\to(1,1)$	−599	2	2	
21	41	$(4,0)\to(1,2)$	−439	2	3	
22	22A	$(2,1)\to(2,0)$	−206	1	3	232
23	22B	$(2,2)\to(2,0)$	−393	2	2	
24	22C	$(2,0)\to(2,0)$	−7	0	4	253
25	22D	$(2,1)\to(2,1)$	−8	2	2	54
26	22E	$(2,1)\to(2,1)$	−7	2	2	54
27	22F	$(2,0)\to(2,1)$	224	1	3	32
28	32A	$(3,1)\to(2,1)$	−293	2	3	
29	32B	$(3,1)\to(2,1)$	−254	2	3	
30	32C	$(3,0)\to(2,1)$	−56	1	4	203
31	42	$(4,0)\to(2,2)$	−159	2	4	207
32	33	$(3,1)\to(3,1)$	−7	2	4	134

TABLE V. The fitted lateral pair interactions (in meV) for an adatom at (f or h) adsorption (E_1, E_2) and at bridge (E_1^*, E_2^*) sites.

E_1	E_2	E_1^*	E_2^*
−307	−215	−316	−101

$$\Delta E_{\mathrm{fh}} = \Delta E_{\mathrm{fh}}^0 + (N_{d_1}^{\mathrm{f}} - N_{d_1}^{\mathrm{h}})E_1 + (N_{d_2}^{\mathrm{f}} - N_{d_2}^{\mathrm{h}})E_2. \quad (8)$$

The parameter ΔE_{fh}^0 can be interpreted as the difference of total energies for an isolated adatom between f and h sites, i.e., $\Delta E_{\mathrm{fh}}^0 = -5$ meV (see Sec. III C 1). The parameters E_1 and E_2 can be viewed as effective pair interactions between the considered adatom and its neighbors belonging to the adisland at distances d_1 and d_2, respectively. Indeed, it can be seen easily that the three shortest lateral distances d_1, d_2, d_3 between a given threefold site and the neighboring threefold sites are $d_1 = a, d_2 = \sqrt{4/3}a, d_3 = \sqrt{7/3}a$ where a is the nn spacing while calculations show that the optimized z coordinate of these sites are almost the same. Thus the effective pair interaction corresponding to d_3 can be neglected since d_3/d_2 is noticeably larger than d_2/d_1.

Let us now consider the energy barriers $E_{\mathrm{f}\to\mathrm{h}}$ and introduce also effective pair interactions. The optimization of the diffusion path reveals that the saddle point is always very close to the bridge (twofold) site, midway between the initial f and final h sites. The three shortest lateral distances d_1^*, d_2^*, d_3^* between a bridge site and the nearest threefold sites are: $d_1^* = \sqrt{13/12}a$, $d_2^* = \sqrt{19/12}a$, $d_3^* = \sqrt{25/12}a$. Even though d_3^*/d_2^* has the same order of magnitude as d_2^*/d_1^*, the effective pair interaction corresponding to d_3^* has been neglected. This is reasonable in view of the other approximations and it will be seen in the following that taking into account only two effective pair interactions $E_1^*(E_2^*)$ at $d_1^*(d_2^*)$ for an adatom at the bridge position leads to satisfactory results.

Consequently, we have adopted the following expression for the energy barriers $E_{\mathrm{f}\to\mathrm{h}}$:

$$E_{\mathrm{f}\to\mathrm{h}} = E_{\mathrm{f}\to\mathrm{h}}^0 + N_{d_1^*}E_1^* + N_{d_2^*}E_2^* - N_{d_1}^{\mathrm{f}}E_1 - N_{d_2}^{\mathrm{f}}E_2. \quad (9)$$

The parameter $E_{\mathrm{f}\to\mathrm{h}}^0$ is the energy barrier for an isolated adatom, i.e., $E_{\mathrm{f}\to\mathrm{h}}^0 = 41$ meV (see Sec. III C 1). The effective pair interactions E_1, E_2, E_1^*, and E_2^* are determined by a least mean square fit of ΔE_{fh} and $E_{\mathrm{f}\to\mathrm{h}}$ given in Table IV. They are given in Table V. The calculated and fitted values of ΔE_{fh} and $E_{\mathrm{f}\to\mathrm{h}}$ are in satisfactory agreement (Figs. 14 and 15). Note, however, that none of the 32 configurations included in the fit has *pn* bonds in the direction of the displacement in the initial or in the final positions, i.e., the diffusing adatom at the bridge position has no neighbor at the distance d_3^*.

Let us now check that our fit gives reasonable estimates of energy differences and barriers not included in the determination of the parameters. We first note that the numerical values of the parameters E_1, E_2, E_1^*, E_2^* are quite reasonable. Indeed E_1 and E_1^* are rather close, similarly to the corresponding distances, whereas E_2^* is smaller than E_2 since $d_2^* > d_2$. For assessing the quality of the fit we have first used this set of parameters to compute the energy barriers $E_{\mathrm{h}\to\mathrm{f}}$ in the reverse direction (with $E_{\mathrm{h}\to\mathrm{f}}^0 = 36$ meV, see Sec. III C 1). The overall agreement (Fig. 15) is rather good. In addition, in order to justify the neglect of E_3^* we have also considered configurations having $N_{d_2^{//}}^{\mathrm{f(h)}}$ pn bonds parallel to the displacement in the initial(final) state $[N_{d_2^{//}}^{\mathrm{f(h)}} = 0, 1$, see Fig. 16]. The full calculations of ΔE_{fh} and $E_{\mathrm{f}\to\mathrm{h}}$ have been carried out using the same assumptions on the adatom relaxation as for the 32 previous configurations. The results are given in Table VI and compared to the fitted values in Fig. 17. The overall agreement is once again quite satisfactory. It is also important to stress that in all cases where no barrier is found, the total energy at the bridge site is in between the initial and final total energies in our fit, as it should.

The success of this effective pair potential approach is actually not completely unexpected. Indeed, such a model has already been justified for the determination of the variation of the surface energy as a function of the crystallographic orientation by detailed calculations based on semiempirical potentials,[47] tight-binding model,[48] and *ab initio* calculations.[49] Note that this does not assume that the total energy of metals can be written as a sum of pair interactions

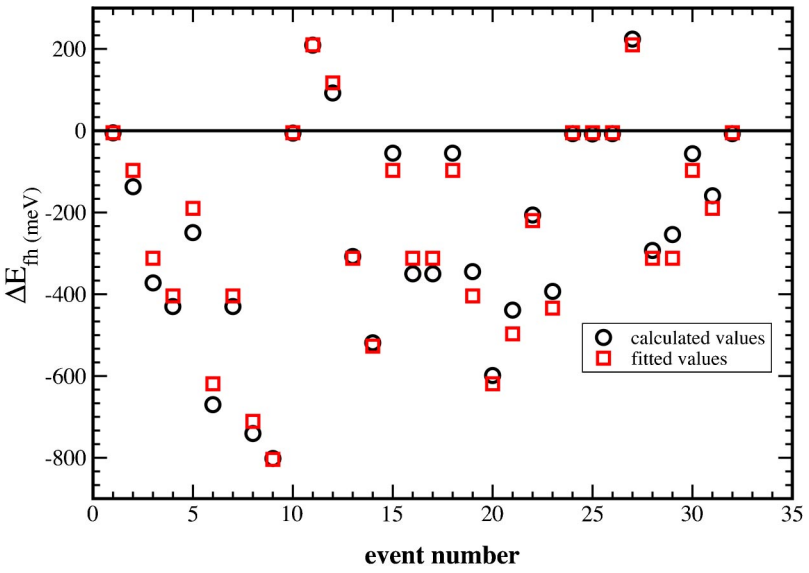

FIG. 14. The calculated (open circles) difference in energy $\Delta E_{\mathrm{fh}} = E_{\mathrm{f}} - E_{\mathrm{h}}$ between f and h adsorption sites and the corresponding fitted values (open squares) for the 32 events presented in Table IV and Fig. 13.

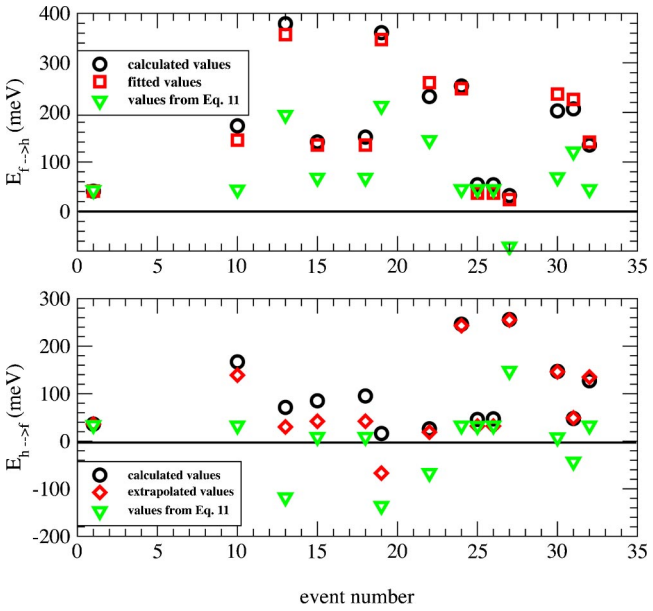

FIG. 15. The activation barriers corresponding to the configurations shown in Fig. 13. The results of the full calculations are denoted as open circles. The open triangles give the values obtained from Eq. (11) (Ref. 24) using the numerical values listed in Table IV. Upper panel: comparison between calculated and fitted (open squares) values of the activation barriers $E_{f\to h}$ for an f to h jump. Lower panel: comparison between calculated and extrapolated (open diamonds) values of the activation barriers $E_{h\to f}$ for an h to f jump.

but that the variation of the total energy due to a modification of the coordinations in a limited range can be linearized.

Finally, let us now compare our results with previous works in the literature. It is often assumed[50,51] that the energy barriers are completely determined by the numbers of nearest neighbors at the initial and final positions. Actually, it is easy to show that

$$N_{d_1^*} = N^{\mathrm{f}}_{d_2} + N^{\mathrm{h}}_{d_2} - N^{\mathrm{f}}_{d_{2//}} - N^{\mathrm{h}}_{d_{2//}},$$

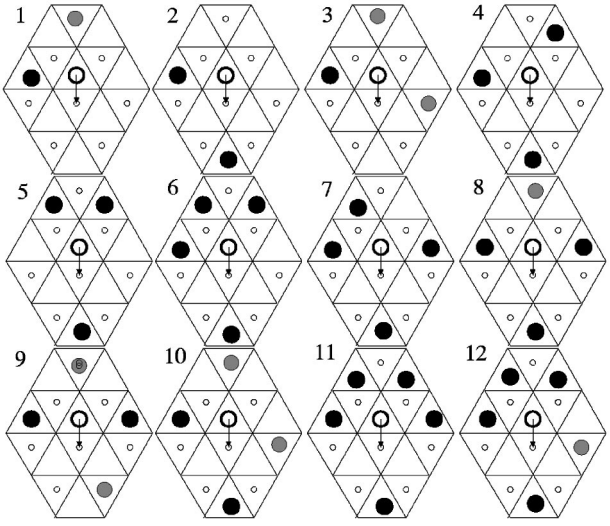

FIG. 16. Same caption as in Fig. 13 for the 12 atomic configurations used as a test of the effective pair interaction model.

TABLE VI. Same caption as Table IV for the 12 configurations drawn in Fig. 16.

No.	$(N^{\mathrm{f}}_{d_1}, N^{\mathrm{f}}_{d_2}) \to (N^{\mathrm{h}}_{d_1}, N^{\mathrm{h}}_{d_2})$	ΔE_{fh}	$N_{d_1^*}$	$N_{d_2^*}$	$E_{\mathrm{f}\to\mathrm{h}}$
1	$(1,1)\to(0,1)$	−309	0	1	
2	$(1,0)\to(0,2)$	121	1	0	41
3	$(1,2)\to(1,1)$	−215	2	0	
4	$(2,0)\to(0,2)$	−225	1	1	261
5	$(2,0)\to(0,1)$	−395	0	2	478
6	$(3,0)\to(0,2)$	−485	1	2	
7	$(3,0)\to(0,3)$	−290	2	1	
8	$(2,1)\to(0,3)$	−230	2	0	230
9	$(2,1)\to(1,2)$	−87	2	1	134
10	$(1,2)\to(1,2)$	−2	2	0	101
11	$(4,0)\to(0,3)$	−543	2	2	
12	$(3,1)\to(1,2)$	−347	2	2	

$$N_{d_2^*} = N^{\mathrm{f}}_{d_1} + N^{\mathrm{h}}_{d_1} - N_{d_1^*}. \tag{10}$$

We see that the above assumption would be justified if only the first nearest neighbor interaction were taken into account. In the present case, however, we have shown that this simple assumption is not valid since pn interactions must be introduced and the pn bonds parallel to the displacement play a peculiar role [see Eq. (10)]. Another simple model has been proposed by Fichthorn *et al.*[24] in which the energy barriers $E_{f\to h}$ are given by

$$E_{\mathrm{f}\to\mathrm{h}} = E^0_{\mathrm{f}\to\mathrm{h}} - \tfrac{1}{2}\Delta E_{\mathrm{fh}}. \tag{11}$$

The energy barriers calculated with the above formula, using the values of ΔE_{fh} listed in Table IV, are given in Fig. 15. The comparison with our full calculations shows that Eq. (11) cannot be used when the diffusing adatom has short range interaction with other adatoms, even though it upholds the detailed balance criterion.

V. CONCLUSION

To summarize, we have carried out a systematic study of the diffusion of Cu on Cu(111), with particular emphasis on the influence of short range adatom-adatom interactions. Using the EAM potential set up by Mishin *et al.*, we have first considered the case of a single adatom. The most stable adsorption site (f) and the very small diffusion barrier are in perfect agreement with experiments. When adatoms meet to form very small clusters (dimers, trimers) we find that these clusters move easily on the surface. However, this movement does not involve bond breaking. Dimers are of three types ff, hh, and fh, ff and fh dimers being almost degenerate in energy. The diffusion barriers are very small for intracell motion whereas intercell motion proceeds by concerted sliding and is less frequent, as predicted by molecular dynamic simulations. The most favorable among the four triangular trimer configurations is 3fA, which is almost degenerate in energy with 3fB. However, all these configurations can be visited by concerted motion at room temperature. The diffu-

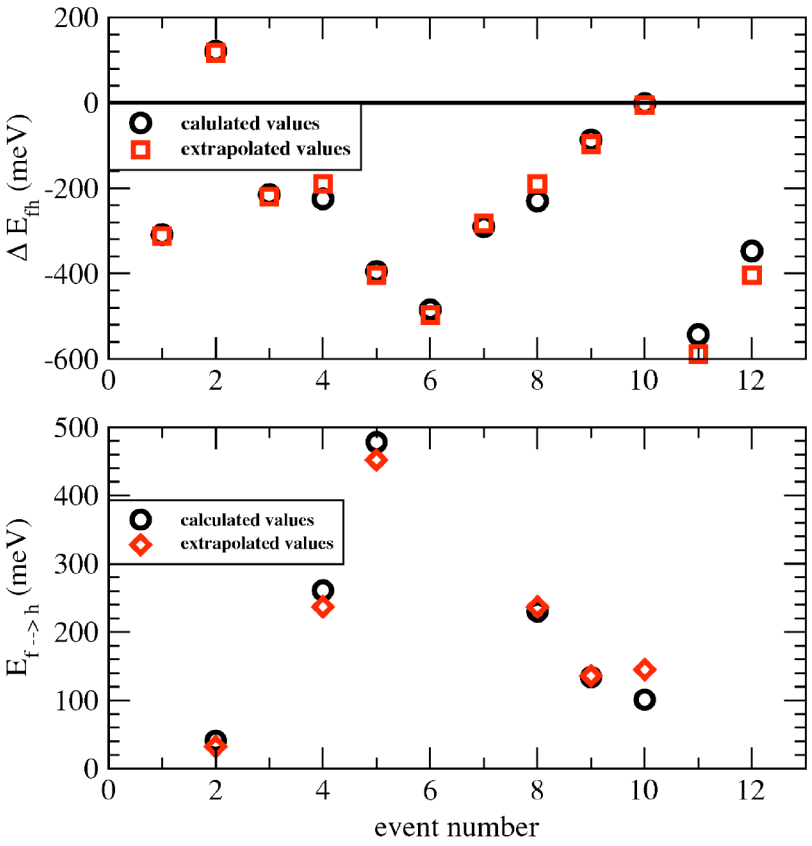

FIG. 17. Upper panel: comparison between calculated (open circles) and extrapolated (open squares) values of the difference in energy $\Delta E_{fh}=E_f-E_h$ between f and h adsorption sites for the 12 configurations shown in Fig. 16. Lower panel: comparison between calculated (open circles) and extrapolated (open diamonds) values of the activation barriers $E_{f\to h}$ for an f to h jump found for the set of configurations shown in Fig. 16.

sion barriers for concerted sliding have also been determined for the close-packed tetramer and heptamer. The Vineyard prefactors have been calculated allowing us to estimate the critical island size beyond which the nuclei can be considered as immobile at a given temperature. In addition the local spectral vibration densities of monomers and dimers have been presented.

Then the influence of the lateral environment of the initial and final sites in the diffusion process has been investigated. Calculations reveal that the existence as well as the height of the diffusion barrier are strongly dependent on this environment. Finally, we have shown that the energy difference between the initial and final configurations can be well estimated using two effective pair interactions corresponding to the two shortest interatomic distances, i.e., to ff and hh bonds, in the one hand, and fh (pseudoneighbor) bond, on the other hand. Similarly, the introduction of effective pair interactions corresponding to the two shortest interatomic distances at the bridge site has allowed us to reproduce and predict the existence and the height of the diffusion barriers.

In conclusion, we have investigated several microscopic aspects that will be of importance to study the homoepitaxial growth on Cu(111). However, the detailed knowledge of the diffusion mechanism of adatoms along straight and kinked close-packed steps is still required. This study is currently in progress and will be published in a forthcoming paper.

ACKNOWLEDGMENTS

We wish to thank Ludovic Douillard and Laurent Proville for fruitful discussions and the referee for interesting suggestions.

[1] M. Villarba and H. Jónsson, Surf. Sci. **317**, 15 (1994).
[2] R. Stumpf and M. Scheffler, Phys. Rev. B **53**, 4958 (1996).
[3] A. Bogicevic, J. Strömquist, and B. I. Lundqvist, Phys. Rev. Lett. **81**, 637 (1998).
[4] S. Ovesson, A. Bogicevic, and B. I. Lundqvist, Phys. Rev. Lett. **83**, 2608 (1999).
[5] K. A. Fichthorn and M. Scheffler, Phys. Rev. Lett. **84**, 5371 (2000).
[6] E. Vamvakopoulos and G. A. Evangelakis, J. Phys.: Condens. Matter **13**, 10757 (2001), and references therein.
[7] D. C. Schlößer, K. Morgenstern, L. K. Verheij, G. Rosenfeld, F. Besenbacher, and G. Comsa, Surf. Sci. **465**, 19 (2000).
[8] M. Giesen and H. Ibach, Surf. Sci. **529**, 135 (2003).
[9] S. C. Wang and G. Ehrlich, J. Chem. Phys. **94**, 4071 (1991); Phys. Rev. Lett. **68**, 1160 (1992).
[10] J. Repp, G. Meyer, K. H. Rieder, and P. Hyldgaard, Phys. Rev. Lett. **91**, 206102 (2003).
[11] B. Piveteau, D. Spanjaard, and M. C. Desjonquères, Phys. Rev. B **46**, 7121 (1992).
[12] S. Papadia, B. Piveteau, D. Spanjaard, and M. C. Desjonquères,

Phys. Rev. B **54**, 14 720 (1996).
[13] P. J. Feibelman, Phys. Rev. Lett. **69**, 1568 (1992).
[14] C. M. Chang, C. M. Wei, and S. P. Chen, Phys. Rev. Lett. **85**, 1044 (2000).
[15] C. Ratsch and M. Scheffler, Phys. Rev. B **58**, 13 163 (1998).
[16] P. J. Feibelman, Phys. Rev. Lett. **85**, 606 (2000).
[17] C. L. Liu, J. M. Cohen, J. B. Adams, and A. F. Voter, Surf. Sci. **253**, 334 (1991).
[18] S. Ovesson, A. Bogicevic, G. Wahnström, and B. I. Lundqvist, Phys. Rev. B **64**, 125423 (2001).
[19] J. V. Barth, H. Brune, B. Fischer, J. Weckesser, and K. Kern, Phys. Rev. Lett. **84**, 1732 (2000).
[20] J. C. Hamilton, M. R. Sørensen, and A. F. Voter, Phys. Rev. B **61**, R5125 (2000).
[21] G. Kress and J. Hafner, Phys. Rev. B **49**, 14251 (1994).
[22] A. Bogicevic, S. Ovesson, P. Hyldgaard, B. I. Lundqvist, H. Brune, and D. R. Jennison, Phys. Rev. Lett. **85**, 1910 (2000).
[23] U. Kürpick, Phys. Rev. B **66**, 165431 (2002).
[24] K. A. Fichthorn, M. L. Merrick, and M. Scheffler, Appl. Phys. A: Mater. Sci. Process. **75**, 17 (2002).
[25] G. Henkelman and H. Jónsson, J. Chem. Phys. **115**, 9657 (2001); Phys. Rev. Lett. **90**, 116101 (2003).
[26] A. F. Voter, F. Montalenti, and T. C. Germann, Annu. Rev. Mater. Res. **32**, 321 (2002).
[27] Y. Mishin, M. J. Mehl, D. A. Papaconstantopoulos, A. F. Voter, and J. D. Kress, Phys. Rev. B **63**, 224106 (2001).
[28] S. A. Lindgren, L. Wallden, J. Rundgren, and P. Westrin, Phys. Rev. B **29**, 576 (1984).
[29] D. M. Lind, F. B. Dunning, G. K. Walters, and H. L. Davis, Phys. Rev. B **35**, 9037 (1987).
[30] D. L. Adams, H. B. Nielsen, and J. N. Andersen, Surf. Sci. **128**, 284 (1983).
[31] D. C. Schlößer, L. K. Verheij, G. Rosenfeld, and G. Comsa, Phys. Rev. Lett. **82**, 3843 (1999).
[32] C. Steimer, M. Giesen, and H. Ibach, Surf. Sci. **471**, 80 (2001).
[33] C. Carter and I. L. F. Ray, Philos. Mag. **35**, 189 (1977).
[34] U. Harten, C. Woll, and J. P. Toennies, Phys. Rev. Lett. **55**, 2308 (1985); B. M. Hall, D. L. Mills, M. H. Mohamed, and L. L. Kesmodel, Phys. Rev. B **38**, 5856 (1988); C. Kaden, P. Ruggerone, J. P. Toennies, G. Zhang, and G. Benedek, *ibid.* **46**, 13 509 (1992).
[35] M. J. Gillan, J. Phys.: Condens. Matter **1**, 689 (1989).
[36] A. Ulitsky and R. Elber, J. Chem. Phys. **92**, 1510 (1990).
[37] M. C. Desjonquères and D. Spanjaard, *Concepts in Surface Physics* (Springer-Verlag, New York, 1993).
[38] M. P. Allen and D. Tildesley, *Simulation of Liquids* (Clarendon, Oxford, 1987).
[39] M. C. Marinica, G. Raşeev, and K. S. Smirnov, Phys. Rev. B **63**, 205422 (2001).
[40] L. Verlet, Phys. Rev. **159**, 98 (1967).
[41] D. I. Blokhintsev, *Mécanique Quantique et Application à la Structure de la Matière* (Masson, Paris, 1967), p. 279.
[42] A. Bogicevic, P. Hyldgaard, G. Wahnström, and B. I. Lundqvist, Phys. Rev. Lett. **81**, 172 (1998).
[43] G. H. Vineyard, J. Phys. Chem. Solids **3**, 121 (1957).
[44] M. Giesen and H. Ibach, Surf. Sci. **431**, 109 (1999).
[45] W. Meyer and H. Neldel, Z. Tech. Phys. (Leipzig) **12**, 588 (1937).
[46] M. C. Marinica, C. Barreteau, D. Spanjaard, and M. C. Desjonquères (unpublished).
[47] Siqing Wei and M. Y. Chou, Phys. Rev. B **50**, 4859 (1994).
[48] F. Raouafi, C. Barreteau, M. C. Desjonquères, and D. Spanjaard, Surf. Sci. **505**, 183 (2002).
[49] I. Galanakis, G. Bihlmayer, V. Bellini, N. Papanikolaou, R. Zeller, S. Blügel, and P. H. Dederichs, Europhys. Lett. **58**, 751 (2002).
[50] M. L. Larsson, Phys. Rev. B **64**, 115428 (2001).
[51] J. M. Pomeroy, J. Jacobsen, C. C. Hill, H. Barbara, and J. P. Sethna, Phys. Rev. B **66**, 235412 (2002).